although the proximal mechanism for these losses remains uncertain. Beyond endangering top predators, warming caused complex changes in trophic structure that altered ecosystem processes, for example, facilitation of primary production resulting from reduced top-down control of producers. Comparable changes in trophic structure and ecosystem processes could shift the carbon budget of natural aquatic ecosystems[26], producing an important feedback between global warming and food-web structure. □

Methods

Microcosms

Microcosms were 250-ml culture bottles containing 100 ml of medium[11] inoculated with either 6–7 (low-diversity) or 13–16 (high-diversity) species of eukaryotic microorganisms. Different combinations of species (Fig. 1) created two types of low-diversity community (Low A and Low B) and two types of high-diversity community (High A and High B). A predator was added to the Low B community but failed to establish. Additions of bacteria (*Serratia marcescens*, *Bacillus subtilis* and *Bacillus cereus* in all microcosms) and other microorganisms were lagged to ensure that consumers were not introduced until their prey became abundant.

Directional environmental change

Half the microcosms experienced warming of +2 °C per week for the first five weeks of the experiment (22–32 °C), constant temperature for the sixth week, and warming to 34 °C at the beginning of the seventh week. The other half remained at 22 °C for the duration of the experiment. Replicates of temperature treatments were housed in four incubators (two constant temperature, two warming) with 16:8 h light:dark cycles to avoid pseudoreplication of temperature regimes.

Community monitoring

Species presence/absence was determined weekly by microscopy. We calculated extinction frequency as (maximum species richness − final species richness)/maximum species richness, because some species grew slowly to detectable densities. No contamination occurred. Population density of each species was estimated during week six by counting the number of individuals in a sample and converting counts to biomass using species-specific estimates of cell mass[27]. Bacterial density was estimated weekly from plate counts.

Primary production

A multichannel closed-circuit respirometer (Columbus Scientific) measured O_2 flux over 4 h with lights on and 4 h with lights off each week. Microcosms were housed in heated and lit water baths during respirometry to maintain temperature treatments. Primary production was O_2 flux rate (light) − O_2 flux rate (dark). Expected values of primary production based on temperature-dependent physiological rates were estimated as $\text{Production}_{\text{expected}} = \text{Production}_{\text{constant}} \times Q_{10} \times (\text{Temperature}_{\text{warmed}} - \text{Temperature}_{\text{constant}})/10$ for each replicate during each week with $Q_{10} = 2$. Deviation of observed from expected production under warming was the difference between observed and expected values on a given date.

Decomposition

We estimated decomposition from the proportion change in dry mass over the first five weeks of preweighed wheat seeds in individually labelled nylon mesh bags[11].

Data analysis

Effects of warming, diversity and composition on extinction frequencies, primary production and decomposition were determined with separate three-way analyses of variance (ANOVAs). Effects of temperature regime and trophic position on extinction frequencies were determined with a two-way ANOVA. Effects of initial diversity, species composition and warming on the biomass of five trophic groups (bacteria, producers, bacterivores, herbivores and predators) were determined with MANOVA. The differences between warming and constant communities in proportions of producers, bacterivores, herbivores and predators quantified the effects of warming on trophic structure, and principal components analysis summarized variation in these four differenced proportion variables. Multiple regression related the deviation in production to changes in trophic structure (the first three PC axes), total number of species and bacterial biomass. Separate logistic regressions tested for relations between extinctions (binary variable) and log (body size), and extinctions and log (abundance) because body size and abundance were tightly correlated ($r^2 = 0.90$).

Received 19 July; accepted 7 September 1999.

1. Frost, T. M., Carpenter, S. R., Ives, A. R. & Kratz, T. K. in *Linking Species and Ecosystems* (eds Jones, C. G. & Lawton, J. H.) 224–239 (Chapman & Hall, New York, 1995).
2. Davis, A. J., Jenkinson, L. S., Lawton, J. H., Shorrocks, B. & Wood, S. Making mistakes when predicting shifts in species range in response to global warming. *Nature* **391,** 783–786 (1998).
3. Sanford, E. Regulation of keystone predation by small changes in ocean temperature. *Science* **283,** 2095–2097 (1999).
4. Harte, J. & Shaw, R. Shifting dominance within a montane vegetation community: results of a climate-warming experiment. *Science* **267,** 876–880 (1995).
5. Parmesan, C. *et al.* Poleward shifts in geographical ranges of butterfly species associated with regional warming. *Nature* **399,** 579–583 (1999).
6. Naeem, S. & Li, S. Biodiversity enhances ecosystem reliability. *Nature* **390,** 507–509 (1997).
7. Yachi, S. & Loreau, M. Biodiversity and ecosystem productivity in a fluctuating environment: the insurance hypothesis. *Proc. Natl Acad. Sci. USA* **96,** 1463–1468 (1999).
8. Ives, A. R. & Gilchrist, G. in *Biotic Interactions and Global Change* (eds Kareiva, P. M., Kingsolver, J. G. & Huey, R. B.) 120–146 (Sinauer Associates Inc., Sunderland, 1993).
9. Houghton, J. T. *et al. Climate Change 1995: The Science of Climate Change* (Cambridge Univ. Press, Cambridge, 1996).
10. Lawton, J. H. Ecological experiments with model systems. *Science* **269,** 328–331 (1995).
11. McGrady-Steed, J., Harris, P. M. & Morin, P. J. Biodiversity regulates ecosystem predictability. *Nature* **390,** 162–165 (1997).
12. May, R. M. *Stability and Complexity in Model Ecosystems* (Princeton Univ. Press, Princeton, 1973).
13. Pimm, S. L. *The Balance of Nature?* (Univ. Chicago Press, Chicago, 1991).
14. Solé, R. V., Manrubia, S. C., Benton, M., Kauffman, S. & Bak, P. Criticality and scaling in evolutionary ecology. *Trends. Ecol. Evol.* **14,** 156–160 (1999).
15. Bak, P. *How Nature Works* (Springer, New York, 1996).
16. Naeem, S. Species redundancy and ecosystem reliability. *Cons. Biol.* **12,** 39–45 (1998).
17. Oksanen, L., Fretwell, S. D., Arruda, J. & Niemelä, P. Exploitation ecosystems in gradients of primary productivity. *Am. Nat.* **118,** 240–261 (1981).
18. Kaunzinger, C. M. K. & Morin, P. J. Productivity controls food-chain properties in microbial communities. *Nature* **395,** 495–497 (1998).
19. Naeem, S. & Li, S. Consumer species richness and autotrophic biomass. *Ecology* **79,** 2603–2615 (1998).
20. Hector, A. The effect of diversity on productivity: detecting the role of species complementarity. *Oikos* **82,** 597–599 (1998).
21. Loreau, M. Separating sampling and other effects in biodiversity experiments. *Oikos* **82,** 600–602 (1998).
22. Hooper, D. U. The role of complementarity and competition in ecosystem responses to variation in plant diversity. *Ecology* **79,** 704–719 (1998).
23. Tilman, D., Lehman, C. L. & Thomson, K. T. Plant diversity and ecosystem productivity: theoretical considerations. *Proc. Natl Acad. Sci. USA* **94,** 1857–1861 (1997).
24. Schindler, D. E., Carpenter, S. R., Cole, J. J., Kitchell, J. F. & Pace, M. L. Influence of food web structure on carbon exchange between lakes and the atmosphere. *Science* **277,** 248–251 (1997).
25. Pounds, J. A., Fogden, M. P. L. & Campbell, J. H. Biological response to climate change on a tropical mountain. *Nature* **398,** 611–615 (1999).
26. Del Giorgio, P. A., Cole, J. J., Caraco, N. F. & Peters, R. H. Linking planktonic biomass and metabolism to net gas fluxes in northern temperature lakes. *Ecology* **80,** 1422–1431 (1999).
27. McGrady-Steed, J. & Morin, P. J. Biodiversity, density compensation and the dynamics of populations and functional groups. *Ecology* (in the press).

Acknowledgements

We thank the NSF for supporting this research. Comments from the Morin lab, J. McGrady-Steed, S. Lawler, M. Loreau and S. Naeem improved the manuscript.

Correspondence and request for materials should be addressed to O.L.P. (e-mail: opetchey@rci.rutgers.edu).

A network of fast-spiking cells in the neocortex connected by electrical synapses

Mario Galarreta & Shaul Hestrin

Department of Anatomy and Neurobiology, University of Tennessee, Memphis, 855 Monroe Avenue, Memphis, Tennessee 38163, USA

Encoding of information in the cortex is thought to depend on synchronous firing of cortical neurons[1,2]. Inhibitory neurons are known to be critical in the coordination of cortical activity[3–5], but how interaction among inhibitory cells promotes synchrony is not well understood[4,6–12]. To address this issue directly, we have recorded simultaneously from pairs of fast-spiking (FS) cells, a type of γ-aminobutyric acid (GABA)-containing neocortical interneuron[13]. Here we report a high occurrence of electrical coupling among FS cells. Electrical synapses were not found among pyramidal neurons or between FS cells and other cortical cells. Some FS cells were interconnected by both electrical and GABAergic synapses. We show that communication through electrical synapses allows excitatory signalling among inhibitory cells and promotes their synchronous spiking. These results indicate that electrical synapses establish a network of fast-spiking cells in the neocortex which may play a key role in coordinating cortical activity.

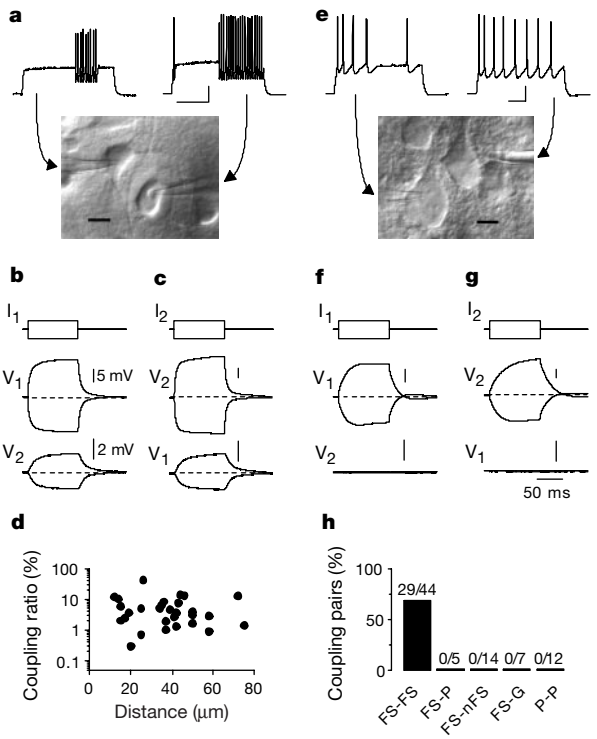

Figure 1 Specific electrical coupling among fast-spiking cells. **a**, Pattern of spiking and IR-DIC video image of two electrically coupled FS cells. **b**, **c**, Simultaneous depolarization or hyperpolarization of two FS cells (V_1, V_2) when positive or negative currents were injected in only one of them (I_1 or I_2). **d**, Coupling ratio versus the distance between the somata of electricity coupled FS cells ($n = 29$). **e**, **f**, **g**, Pairs of neighbouring pyramidal neurons were not electrically coupled. **h**, FS cells were only electrically coupled to other FS cells. FS, fast-spiking cells; P, pyramidal cells; nFS, non-FS nonpyramidal cells; G, glial cells. Scale: **a**, **e**, vertical 20 mV, horizontal 100 ms (spiking pattern), horizontal 10 μm (IR-DIC image); **c**, **f**, **g** as in **b**.

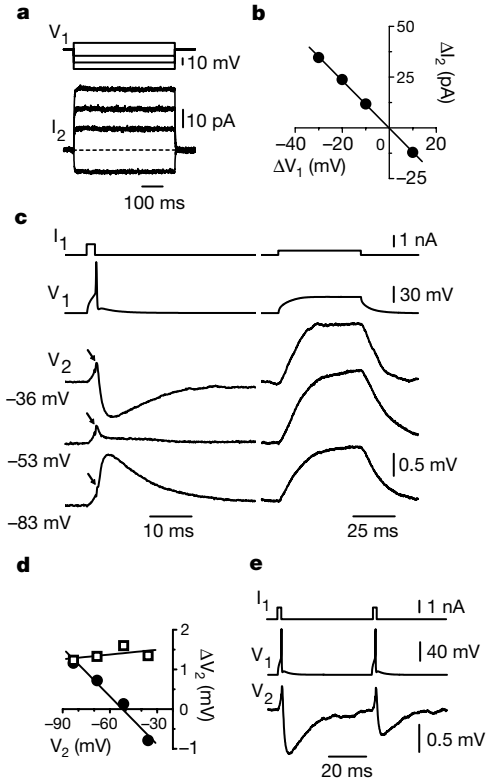

Figure 2 GABA-mediated synaptic transmission and electrical coupling among FS cells. **a**, **b** Example of the current (I_2) recorded from an FS cell when stepping the voltage (V_1) of another FS cell. The estimated conductance of this electrical connection was 1.17 nS. **c**, **d**, Different voltage-dependence of GABA-mediated uIPSPs (filled circles) and electrical transmission (open squares) in a pair of FS cells connected by both electrical and chemical synapses. **e**, Paired-pulse depression of the uIPSPs between the same pair of FS cells as in **c**.

We recorded simultaneously from pairs of fast-spiking non-pyramidal cells (FS cells) in brain slices (Fig. 1a). Fast-spiking cells in layer V were identified on the basis of their characteristic pattern of spiking in response to current injection[14–17] (Fig. 1a; see Methods). Additionally, we found that FS cells showed, in most cases, parvalbumin immunoreactivity[14,18] and had a local axonal projection and aspiny radial dendrites. After identifying a pair of FS cells we tested their electrical coupling under current-clamp or voltage-clamp conditions. Under current-clamp conditions, hyperpolarization of one of the neurons (V_1 in Fig. 1b) by injecting current into this cell (I_1) produced a simultaneous hyperpolarization of the non-injected neuron (V_2 in Fig. 1b). Similarly, depolarizing cell 1 produced a depolarization in cell 2. As expected for electrotonic propagation, voltage deflections recorded in the non-injected neuron had a smaller amplitude and slower time course than those in the injected cell. In all cases, electrical transmission was found to be reciprocal (Fig. 1c). We found that the frequency of coupling among FS cells was 66% (29 of 44 pairs tested, somata less than 80 μm apart). The coupling ratio, estimated as the ratio of the amplitude of the voltage change in the non-injected cell to that in the injected cell, had a mean of 6.4 ± 1.7% (Fig. 1d; range: 0.3–41.1%, $n = 29$). In three further experiments with pairs of FS cells separated by 170–270 μm, one pair was also found to be electrically coupled (coupling ratio: 1.4%).

Electrical coupling appears to be a cell-type specific feature. We found no evidence of electrical coupling among pairs of neighbouring pyramidal neurons (Fig. 1e–g; average distance: 21.4 ± 1.5 μm, $n = 12$ cells). Also, we have not observed electrical coupling in experiments where dual recordings between FS cells and other types of cells were established ($n = 26$). These observations (Fig. 1h) included simultaneous recordings of FS cells and other types of nonpyramidal cells (non-FS nonpyramidal cells, $n = 14$), FS cells and pyramidal cells ($n = 5$), and FS cells and glial cells ($n = 7$).

To estimate the conductance between electrically coupled FS cells we used voltage-clamp conditions[19]. The membrane potential of both FS cells was initially held at −60 mV. We then measured the current produced in cell 2 following a range of voltage commands at cell 1 (Fig. 2a). The conductance between coupled cells was non-rectifying at the membrane potentials tested (Fig. 2b) and its mean amplitude was 658 ± 175 pS ($n = 20$; range: 30–3364 pS). The time course of the current recorded in the coupled neuron was fitted with an exponential function whose time constant ranged from 1.2 ms to 18.5 ms (mean: 6.2 ± 1.4 ms, $n = 20$ pairs). This wide range suggests that electrical contacts occur at different electrotonic distances. In addition, in some pairs we observed that the coupling time constant was significantly faster than the effective input time constant of both cells ($n = 11$ pairs), indicating that in these pairs electrical contacts may occur at proximal locations.

Eight of 44 (18%) pairs of FS cells were connected via GABA-mediated synaptic transmission. Two of these pairs were reciprocally connected and all the pairs connected by GABAergic synapses were also electrically coupled. The time course of the unitary inhibitory postsynaptic potential (uIPSP) had an exponential decay time constant of 10.4 ± 2.0 ms ($n = 7$) and exhibited paired-pulse depression[10] at an interstimulus interval of 50 ms (uIPSP2/uIPSP1 = 0.74 ± 0.03, $n = 7$; Fig. 2e). The average conductance produced by the inhibitory postsynaptic currents (IPSCs) was 1.7 ± 0.4 nS ($n = 4$). When both chemical and electrical transmission were present between two FS cells, a presynaptic spike generated a dual component response in the postsynaptic

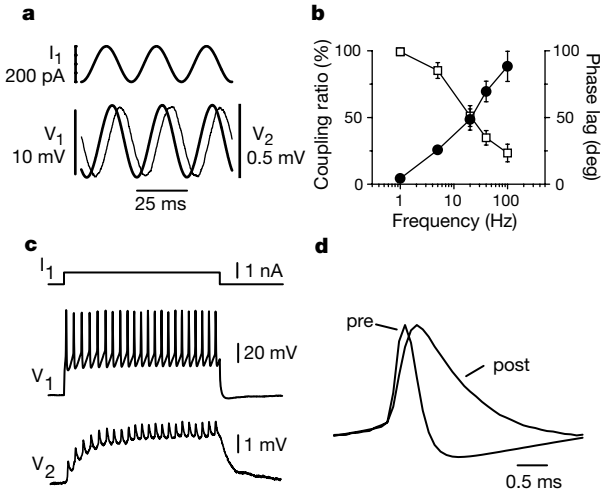

Figure 3 Electrical coupling behaving as a low-pass filter. **a**, Phase lag (62°) between the membrane voltage oscillations produced in a pair of electrically coupled FS cells (V_1 and V_2) when injecting a sine wave current (40 Hz) in one of them (I_1). **b**, Frequency dependence of sine wave transmitted through electrical synapses ($n = 3$–6). Coupling ratios are percentages of the DC signals. Squares, coupling ratio; circles, phase lag. **c**, Example of the electrotonic transmission of a train of action potentials between two coupled FS cells. **d**, Scaled superimposition of a presynaptic spike ('pre') and the corresponding response in the coupled cell ('post').

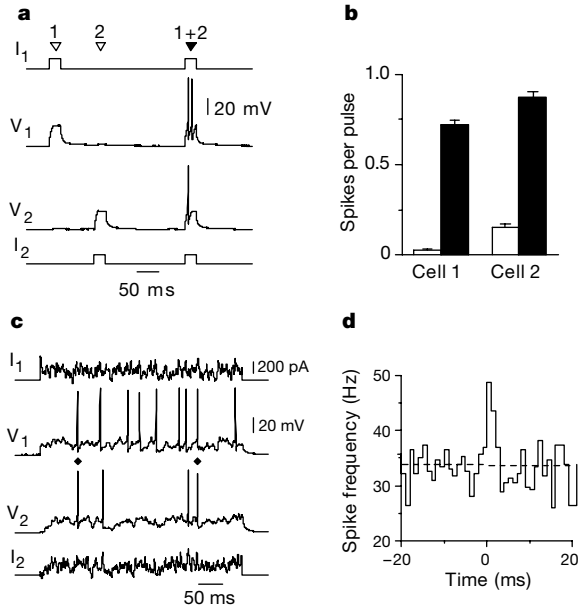

Figure 4 Electrical coupling promoting simultaneous spiking. **a**, Synchronous injection (filled triangle) of subthreshold current pulses (open triangles) in two electrically-coupled FS cells increases the likelihood of firing. Traces represent single trials. **b**, Averaged data ($n = 264$ trials) from the same experiment as in **a**. White bars, non synchronized pulses; black bars, synchronized pulses. **c**, Two electrically coupled FS-cells were injected with uncorrelated synthetic random currents. Diamonds indicate spikes occurring in both cells within a 1-ms window. Traces are single trials. **d**, Normalized cross-correlogram analysis of the pair of cells shown in **c** ($n = 918$ trials). Bin size is 1 ms. Spike frequency is increased near 0 ms.

cell (Fig. 2c). The electrotonic signal consisted of an initial slow response reflecting the subthreshold depolarization of the 'presynaptic' cell, followed by a brief transient signal reflecting the presynaptic spike (Fig. 2c, arrows). When the membrane potential of the postsynaptic cell was maintained at −35 to −40 mV, the $GABA_A$-receptor mediated IPSP was hyperpolarizing whereas the electrotonic component was depolarizing (Fig. 2c and d). The peak of the electrotonic depolarization occurred earlier than that of the $GABA_A$-receptor mediated IPSP. Near the reversal potential of the IPSP only a depolarizing electrotonic component was apparent (Fig. 2c and d). At a more hyperpolarized potential both chemical and electrotonic signals were depolarizing (Fig. 2c and d).

We found that the efficacy of signal transmission through electrical coupling is frequency-dependent. We injected sinusoidal current waveforms into an FS cell and measured the response in the coupled cell (Fig. 3a). Responses to low-frequency sine waves showed larger coupling ratios and smaller phase lags than those induced by high-frequency sine waves (Fig. 3b). This frequency-dependent attenuation resulted in a smaller coupling ratio of action potentials compared with the coupling ratio of DC signals (1.4% and 10%, respectively; $n = 10$). When a train of spikes was generated in an FS cell (Fig. 3c), the response in the coupled cell consisted of a slow and relatively large response to the DC component of the spike train and smaller transient responses corresponding to each action potential (Fig. 3c). The average latency between the peak of a presynaptic spike (pre) and the peak of its corresponding response in the coupled cell (post) was 0.34 ± 0.02 ms ($n = 10$, Fig. 3d).

Next, we investigated whether electrical coupling among individual FS cells could facilitate simultaneous spiking. To address this issue, a close-to-threshold depolarizing current pulse was injected at different times in two electrically coupled FS cells (Fig. 4a, open triangles 1 and 2). In most cases, these asynchronous pulses did not generate an action potential in either neuron. However, when the same current pulses were synchronously injected in both cells, the two neurons reached spike threshold (Fig. 4a, filled triangle 1 + 2; Fig. 4b). Similar observations were obtained in four pairs of electrically coupled FS cells whose coupling ratios ranged from 4.4% to 41.0%. These results indicate that electrical coupling can promote action potential generation. We also wanted to determine whether electrical coupling could facilitate synchronous spiking in response to a 'natural' stimulus. *In vivo* the activity of cortical neurons is ongoing[20]; therefore, neurons are bombarded with both excitatory and inhibitory postsynaptic currents (EPSCs and IPSCs) at high frequency. We simulated natural activity by injecting two electrically coupled cells with uncorrelated random signals obtained by convolving Poisson trains and previously recorded EPSC and IPSC waveforms (Fig. 4a; see Methods). A cross-correlogram of action potentials evoked in these cells showed a significant ($P < 0.05$) increase in firing frequency centred close to 0 ms (Fig. 4d; $n = 4$ pairs). Rapid electrical transmission of action potentials among individual cells can thus produce precise (within 1 ms) coherent spiking in response to uncorrelated excitation.

Our data indicate that electrical synapses establish a functional network of specific inhibitory neurons within the neocortex. Previously, dye coupling was observed among neocortical interneurons[9,21,22], and anatomical studies observed gap junctions between nonpyramidal cells[23,24]. The frequency dependence of electrical coupling suggests that effective transmission of action potentials will be limited to relatively small domains, whereas slow subthreshold waveforms could spread through larger numbers of electrically coupled FS cells. However, active propagation of spikes to the site of the electrical contact could result in a more efficient transmission than that predicted for passive high-frequency signals. *In vivo* and *in vitro* experiments[4,12,25,26] have suggested that networks of inhibitory neurons are crucial in synchronizing neuronal activity. This proposal has been supported by theoretical models[4,7,27–29]; however, synchronization depended on specific constraints[27–29] when interneurons are interconnected by GABAergic synapses only. We propose that the existence of electrical coupling among inhibitory neurons, demonstrated here, may provide an additional mechanism that will facilitate precisely synchronous spiking of these cells and contribute to the control of activity in the cortex. □

Methods

Parasagittal cortical slices (300 μm thick, 30 degree angle) were obtained from Wistar rats (14–18 days old). Within this range, no correlation was found between the likelihood of coupling among FS cells and the animal age. The extracellular solution bathing the slices was kept at 32–33 °C and contained 125 mM NaCl, 2.5 mM KCl, 1.25 mM NaH_2PO_4, 1 mM $MgSO_4$, 2 mM $CaCl_2$, 26 mM $NaHCO_3$, 20 mM glucose, pH 7.4 (315 mOsm), and was continuously bubbled with a gas mixture of 95% O_2 and 5% CO_2.

Cell identification

Cells were selected and identified based on their physiology as well as their immunocytochemistry and morphology. Cells in layer V of the somatosensory and the visual cortices were initially selected according to their morphology using infrared differential interference contrast (IR-DIC) optics. Neurons lacking an apical dendrite with multipolar appearance were selected as FS cell candidates. To distinguish FS cells from other types of non-FS nonpyramidal cell we examined their response to near-threshold current injection. The distinguishing feature that we used to classify FS cells was the generation of high-frequency non-accommodating discharges of action potentials in response to near-threshold current injection[14–17]. We found that in FS cells ($n = 52$ cells), the mean interspike interval (ISI) in these near-threshold discharges was 8.0 ± 0.7 ms (range 2–23.7 ms), the coefficient of variation of the ISI was 0.085 ± 0.007, and the ratio of the second ISI to the first was 1.08 ± 0.02. Nonpyramidal neurons that lacked these characteristic discharges were classified as non-FS nonpyramidal cells. In this group, near-threshold discharges containing ⩾3 spikes had a mean ISI of 62.3 ± 10.8 ms (range 31.6–161.8), a coefficient of variation of the ISI of 0.483 ± 0.096, and a ratio of the second ISI to the first of 3.21 ± 1.00 ($n = 13$). FS cells also had the following characteristics: input resistance 92.4 ± 4 MΩ ($n = 52$), input time constant 8 ± 0.7 ms (measured by fitting the late phase of the response to a small current injection, $n = 50$), fast afterhyperpolarization amplitude −21.7 ± 0.6 mV (measured from the spike onset, $n = 52$), and spike width at threshold 0.6 ± 0.02 ms ($n = 52$). In addition, FS cells exhibited a remarkably high activity of spontaneous excitatory postsynaptic potentials (EPSPs). Pyramidal neurons were recognized by their characteristic morphology and pattern of spiking[16]. Glial cells were identified as having a resting potential more hyperpolarized than −80 mV, low input resistance, absence of synaptic inputs and inability to generate action potentials.

Morphology of neurons stained with biocytin was revealed by standard avidin-biotinylated-horseradish peroxidase complex (ABC, Vector Laboratories) and 3-3′ diaminobenzidine reaction. Fast-spiking cells successfully recovered were nonpyramidal neurons with aspiny radial dendrites. The axon originated in most cases from the upper part of the soma and branched locally with a predominantly horizontal orientation. Immunofluorescence methods were used to detect the presence of parvalbumin in biocytin-stained cells. We used mouse monoclonal antibodies against parvalbumin (Swant, #235, 1/5000), and secondary mouse IgG antibodies (Fab specific) conjugated with TRITC (tetramethylhodamineisothiocyanate) (Sigma, T-7782, 1/400). Biocytin-filled cells were detected using Neutravidin-Alexa 488 (Molecular Probes). Nine of twelve (75%) neurons classified as FS cells were immunopositive for parvalbumin. In contrast, none of ten non-FS cells tested for parvalbumin were immunopositive.

Recording and data analysis

Simultaneous somatic whole-cell recordings (Axopatch 200 A/B; Axon Instruments) were made using patch pipettes (2–4 MΩ) filled with a solution containing 130 mM K-methylsulphate, 6.3 mM KCl, 10 mM HEPES, 4 mM MgATP, 20 mM phosphocreatine(Na), 0.3 mM NaGTP, 10 mM EGTA and 0.3% mM biocytin, (pH 7.3, 295 mOsm). The liquid junction potential error was not corrected. The error in the estimation of the conductance between coupled cells produced by the series resistances was corrected[19]. Recordings from pairs of FS cells were obtained in the presence of DNQX (10 μM, RBI) to block AMPA/kainate receptor-mediated synaptic currents. Chemical synaptic transmission was studied by generating action potentials in the presynaptic neuron using brief pulses (3–5 ms) of suprathreshold currents. The reversal potential of the uIPSP was −56 mV ($n = 4$) and 10 μM bicuculline methiodide (a $GABA_A$-receptor antagonist) blocked the uIPSP generated by FS cells ($n = 3$). Voltage and current signals were filtered at 10 kHz and digitized at 16-bit resolution (National Instruments). The sampling frequency was 5–10 kHz. To synthesize 'natural' stimuli we convolved a Poisson train (2,000 Hz) with a waveform of an excitatory postsynaptic current (EPSC). The result was combined with the convolution of a Poisson train (1,000 Hz) and an IPSC waveform[30]. Trials were separated by 1 s. For each trial a different randomly generated Poisson train was used. The waveforms of the EPSC and IPSC used in the convolution were previously recorded unitary currents.

Data are given as mean ± s.e.m. Statistical analysis testing two-sample hypothesis was performed using unpaired, two-tailed Student's t tests. Differences were considered statistically significant if $P \leqslant 0.05$. Peaks in the cross-correlogram were considered significant if individual bins exceeded expected value by 2.5 standard deviations.

Received 27 April; accepted 23 August 1999.

1. Singer, W. & Gray, C. M. Visual feature integration and the temporal correlation hypothesis. *Annu. Rev. Neurosci.* **18,** 555–586 (1995).
2. Ritz, R. & Sejnowski, T. J. Synchronous oscillatory activity in sensory systems: new vistas on mechanisms. *Curr. Opin. Neurobiol.* **7,** 536–546 (1997).
3. Lytton, W. W. & Sejnowski, T. J. Simulations of cortical pyramidal neurons synchronized by inhibitory interneurons. *J. Neurophysiol.* **66,** 1059–1079 (1991).
4. Whittington, M. A., Traub, R. D. & Jefferys, J. G. R. Synchronized oscillations in interneuron networks driven by metabotropic glutamate receptor activation. *Nature* **373,** 612–615 (1995).
5. Cobb, S. R., Buhl, E. H., Halasy, K., Paulsen, O. & Somogyi, P. Synchronization of neuronal activity in hippocampus by individual GABAergic interneurons. *Nature* **378,** 75–78 (1995).
6. Michelson, H. B. & Wong, R. K. S. Synchronization of inhibitory neurones in the guinea-pig hippocampus in vitro. *J. Physiol. (Lond.)* **477,** 35–45 (1994).
7. Jefferys, J. G. R., Traub, R. D. & Whittington, M. A. Neuronal networks for induced '40 Hz' rhythms. *Trends Neurosci.* **19,** 202–208 (1996).
8. Strata, F. *et al.* A pacemaker current in dye-coupled hilar interneurons contributes to the generation of giant GABAergic potentials in developing hippocampus. *J. Neurosci.* **17,** 1435–1446 (1997).
9. Benardo, L. S. Recruitment of GABAergic inhibition and synchronization of inhibitory interneurons in rat neocortex. *J. Neurophysiol.* **77,** 3134–3144 (1997).
10. Tamás, G., Somogyi, P. & Buhl, E. H. Differentially interconnected networks of GABAergic interneurons in the visual cortex of the cat. *J. Neurosci.* **18,** 4255–4270 (1998).
11. Rinzel, J., Terman, D., Wang, X.-J. & Ermentrout, B. Propagating activity patterns in large-scale inhibitory neuronal networks. *Science* **279,** 1351–1355 (1998).
12. Zhang, Y. *et al.* Slow oscillations (≤1 Hz) mediated by GABAergic interneuronal networks in rat hippocampus. *J. Neurosci.* **18,** 9256–9268 (1998).
13. Kawaguchi, Y. & Kubota, Y. GABAergic cell subtypes and their synaptic connections in rat frontal cortex. *Cereb. Cortex* **7,** 476–486 (1997).
14. Kawaguchi, Y. & Kubota, Y. Correlation of physiological subgroupings of nonpyramidal cells with parvalbumin- and calbindinD28k-immunoreactive neurons in layer V of rat frontal cortex. *J. Neurophysiol.* **70,** 387–396 (1993).
15. Kawaguchi, Y. Physiological subgroups of nonpyramidal cells with specific morphological characteristics in layer II/III of rat frontal cortex. *J. Neurosci.* **15,** 2638–2655 (1995).
16. Galarreta, M. & Hestrin, S. Frequency-dependent synaptic depression and the balance of excitation and inhibition in the neocortex. *Nature Neurosci.* **1,** 587–594 (1998).
17. Angulo, M. C., Staiger, J. F., Rosier, J. & Audinat, E. Developmental synaptic changes increase the range of integrative capabilities of an identified excitatory neocortical connection. *J. Neurosci.* **19,** 1566–1576 (1999).
18. Cauli, B. *et al.* Molecular and physiological diversity of cortical nonpyramidal cells. *J. Neurosci.* **17,** 3894–3906 (1997).
19. Neyton, J. & Trautmann, A. Single-channel currents of an intercellular junction. *Nature* **317,** 331–335 (1985).
20. Hubel, D. H. Single unit activity in striate cortex of unrestrained cats. *J. Physiol.* **147,** 226–238 (1959).
21. Connors, B. W., Benardo, L. S. & Prince, D. A. Coupling between neurons of the developing rat neocortex. *J. Neurosci.* **3,** 773–782 (1983).
22. Peinado, A., Yuste, R. & Katz, L. C. Extensive dye coupling between rat neocortical neurons during the period of circuit formation. *Neuron* **10,** 103–114 (1993).
23. Sloper, J. J. Gap junctions between dendrites in the primate neocortex. *Brain Res.* **44,** 641–646 (1972).
24. Katsumaru, H., Kosaka, T., Heizmann, C. W. & Hama, K. Gap junctions on GABAergic neurons containing the calcium-binding protein parvalbumin in the rat hippocampus (CA1 region). *Exp. Brain Res.* **72,** 363–370 (1988).
25. Bragin, A. *et al.* Gamma (40–100 Hz) oscillation in the hippocampus of the behaving rat. *J. Neurosci.* **15,** 47–60 (1995).
26. Buhl, E. H., Tamás, G. & Fisahn, A. Cholinergic activation and tonic excitation induce persistent gamma oscillations in mouse somatosensory cortex in vitro. *J. Physiol. (Lond.)* **513,** 117–126 (1998).
27. Wang, X.-J. & Buzsáki, G. Gamma oscillation by synaptic inhibition in a hippocampal interneuronal network model. *J. Neurosci.* **16,** 6402–6413 (1996).
28. Traub, R. D., Whittington, M. A., Stanford, I. M. & Jefferys, J. G. R. A mechanism for generation of long-range synchronous fast oscillations in the cortex. *Nature* **383,** 621–624 (1996).
29. Bush, P. & Sejnowski, T. Inhibition synchronizes sparsely connected cortical neurons within and between columns in realistic networks models. *J. Comput. Neurosci.* **3,** 91–110 (1996).
30. Stevens, C. F. & Zador, A. M. Input synchrony and the irregular firing of cortical neurons. *Nature Neurosci.* **1,** 210–217 (1998).

Acknowledgements

We thank M. Chang for technical assistance. S.H. was supported by an NIH grant.

Correspondence and requests for materials should be addressed to S.H. (e-mail: shaul@nb.utmem.edu).

Two networks of electrically coupled inhibitory neurons in neocortex

Jay R. Gibson*, Michael Beierlein* & Barry W. Connors

Department of Neuroscience, Division of Biology & Medicine, Brown University, Providence, Rhode Island 02912, USA
** These authors contributed equally to this work*

Inhibitory interneurons are critical to sensory transformations, plasticity and synchronous activity in the neocortex[1,2]. There are many types of inhibitory neurons, but their synaptic organization is poorly understood. Here we describe two functionally distinct inhibitory networks comprising either fast-spiking (FS) or low-threshold spiking (LTS) neurons. Paired-cell recordings showed that inhibitory neurons of the same type were strongly interconnected by electrical synapses, but electrical synapses between